



The CO₂-induced sensible heat changes over the Tibetan Plateau from November to April

Xia Qu^{1,2} · Gang Huang^{2,4,5} · Lihua Zhu³

Received: 24 January 2019 / Accepted: 1 July 2019 / Published online: 4 July 2019
© Springer-Verlag GmbH Germany, part of Springer Nature 2019

Abstract

Based on the monthly outputs of the Couple Model Intercomparison Project phase 5 (CMIP5), the present study examines the contributions of direct and indirect effects of CO₂ to the response of the sensible heat (SH) over the Tibetan Plateau (TP). Under global warming, the TP SH features an uniform increase during November–April (NDJFMA). During NDJFMA, the SH change over the TP can be mainly attributed to the uniform SST increase induced by CO₂ increasing. This uniform SST increase warms the atmosphere. In turn, it leads to: (1) reduction in snowfall over the TP, with maximum over south TP; (2) increased snowmelt mainly above 3000 m and decreased snowmelt near or south of 3000 m elevation south of TP. The net effects of snowfall and snowmelt are towards the reduction of the snow cover over the TP, which may alter the snow-albedo feedback. Consequently, more solar radiation is absorbed by the TP surface, and the TP surface warms. The surface–air temperature difference increases, which leads to the increase in SH. In addition, the enhancement of the SH offsets the increase in absorbed solar radiation and balances the radiation budget. On the above processes, the SST pattern slightly cancels out the TP SH increase; the contributions of CO₂ direct radiative effect and residual terms are relatively small. Over the grids with elevations no less than 3000 m, the averaged changes are generally linear.

Keywords The Tibetan Plateau · Sensible heat · Surface–air temperature difference · Snow cover

1 Introduction

The Tibetan Plateau (TP) is a huge plateau over the Asian continent. Its elevated heating makes the surrounding climate unique across the globe (Li and Yanai 1996). In northern summer, collaborating with the insulating effect of the Himalayas, the TP sensible heating (SH) gives rise to the ascendance-rainfall feedback over South Asia, playing a significant role in the formation of the South Asia monsoon rainfall (Boos and Kuang 2010; Wu et al. 2012). The resultant warm atmosphere south of the TP collaborates with mid-troposphere westerlies and generates warm horizontal temperature advection, which is an important environmental forcing of the Meiyu-bairu rainbelt (Sampe and Xie 2010). The TP heating enhances the southwesterly at a lower level over East Asia, bringing moisture and making East Asia a monsoon domain—the most poleward monsoon domain on earth (Liu et al. 2007; Lee et al. 2015; Wang and Ding 2008). Among the above heating effects, the SH plays a significant role. The TP is the source of many great rivers (such as the Yangtze River). It is called the “water tower” of Asia. In this sense, the modulation of climate over the TP may be

✉ Xia Qu
quxia@mail.iap.ac.cn

- ¹ Center for Monsoon System Research, Institute of Atmospheric Physics, Chinese Academy of Sciences, P. O. Box 9804, Beijing 100029, China
- ² State Key Laboratory of Numerical Modeling for Atmospheric Sciences and Geophysical Fluid Dynamics, Institute of Atmospheric Physics, Chinese Academy of Sciences, Beijing 100029, China
- ³ School of Atmospheric Sciences/Plateau Atmosphere and Environment Key Laboratory of Sichuan Province/Joint Laboratory of Climate and Environment Change, Chengdu University of Information Technology, Chengdu 610225, China
- ⁴ Laboratory for Regional Oceanography and Numerical Modeling, Qingdao National Laboratory for Marine Science and Technology, Qingdao 266237, China
- ⁵ University of Chinese Academy of Sciences, Beijing 100049, China

of great hydrological significance. SH is a component of surface energy transport over the TP, and the change in the SH may influence the surface energy balance. Therefore, we need to pay attention to the SH over the TP.

The SH over the TP features a distinct annual cycle. Figure 1 displays the climatological SH of the CMIP5 multi-model ensemble, which is consistent with observational results in Li et al. (2003) and Wang et al. (2013). In winter, as the large snow cover over the TP leads to large albedo and small solar radiation received by the surface, the SH is the smallest of the year; The climatological SH over north and east TP is below zero, and those for other areas are positive (Fig. 1a, l). In spring, the enhanced solar radiation and resultant snow melt lead to rapid surface warming over the TP. Accompanied by large surface winds, the SH intensifies and spring thus has the largest SH among all the seasons (Fig. 1c–e). The intensification makes the TP transit from a heat sink to heat source, enlarges the thermal contrast

between land and ocean and influences the monsoon onset. In summer, the spatial pattern of the SH over the TP is similar to that of spring, except that the spatial homogeneity is slightly weaker (Fig. 1f–h). Except for the western TP, the rainfall over the TP results in the drop in SH. In autumn, the weakening of solar radiation reduces the surface temperature as well as the SH (Fig. 1i–k).

The concentration of the CO₂ in the atmosphere has been increasing, leading to an increase in earth surface temperature and exerting profound influence on climate (Stocker et al. 2013). From 1980 to 2008, a decreasing trend in SH was found in observational data mainly over the central and eastern TP (Duan and Wu 2010; Zhu et al. 2017). It is attributed to the deceleration of the surface wind. As global mean temperature rises, over the Eurasian continent, mid- and high-latitude warming is larger than tropical and subtropical warming, leading to a weaker thermal contrast in the meridional direction. It resulted in the weakening of westerly

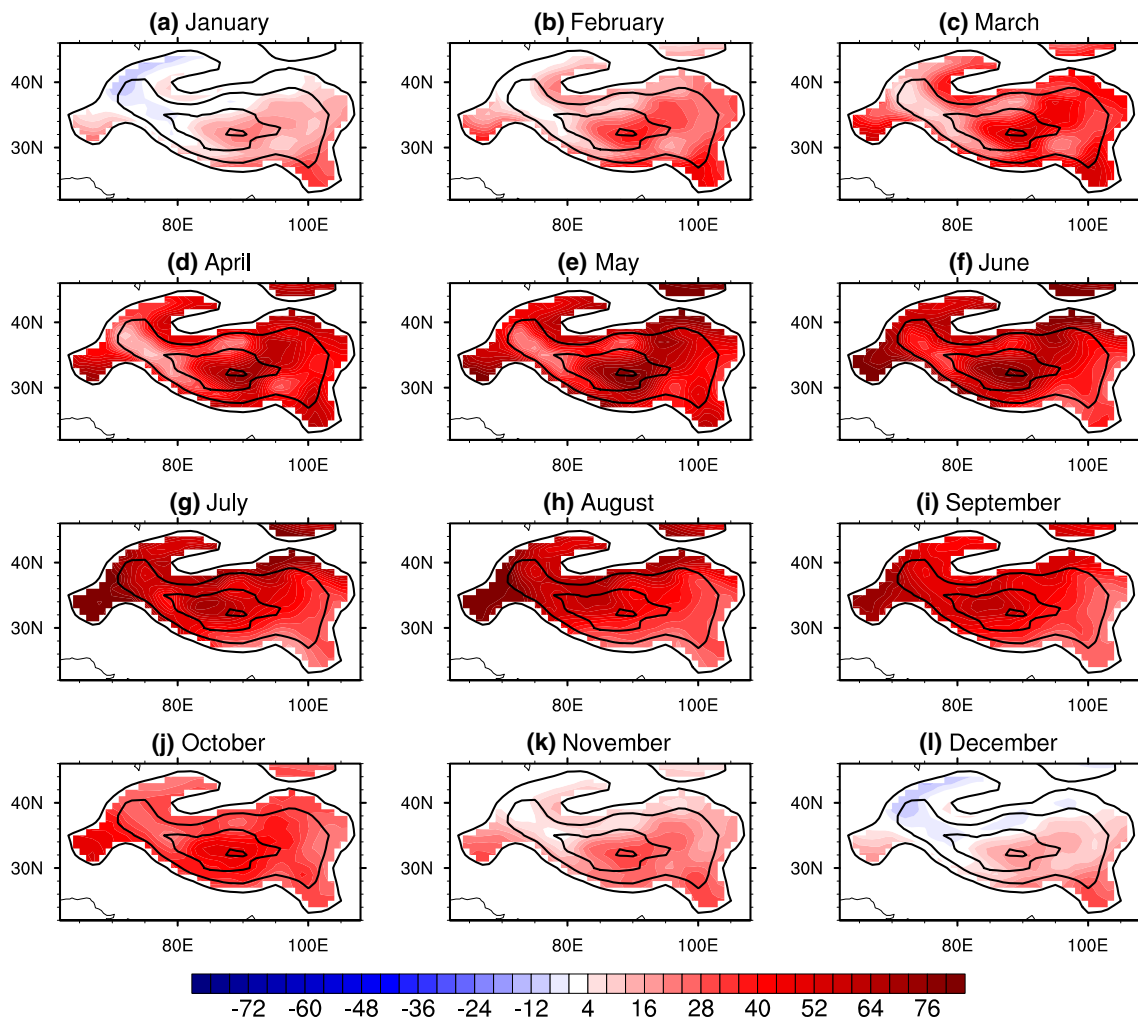


Fig. 1 The climatological SH (color shading) for the historical results (year 1980–2005) in each calendar month. The units are $W m^{-2}$. The results are the MME mean. The contours represent elevations of 1500 m, 3000 m, 5000 m and 6000 m

and surface winds over the TP. As the observational results are the combined effects of the anthropogenic and natural forcing, the contribution of CO₂ alone is hard to understand.

The effects of the increasing CO₂ on the atmosphere can be mainly divided into two kinds of effects. One is the direct effect, which is also called “fast response”. The increasing CO₂ leads to an enhancement of downwards radiation and the increase in land surface temperature as well as the modulations of the other climate variables (Kamae et al. 2015; Sherwood et al. 2015). The other is the indirect effect, also called “slow response”. That is, the increase of CO₂ radiative forcing warms the ocean surface, possibly in turn warming the local atmosphere, or it influences the nonlocal climate via dynamic and thermodynamic processes. Regarding the direct and indirect effects of CO₂, studies focus on their effects on tropical circulations (Bony et al. 2013; Ma et al. 2012), land–sea thermal contrast (Kamae et al. 2014), summertime Asia–Pacific circulation (Shaw and Voigt 2015) and monsoon behavior (Li and Ting 2017; Endo et al. 2018). Taking the Asia monsoon rainfall as an example, using Couple Model Intercomparison Project phase 5 (CMIP5) experiments, Li and Ting (2017) and Endo et al. (2018) found that under a scenario of increasing CO₂, the direct effect enhances the thermal contrast between land and ocean, strengthens the moisture convergence over the Asia monsoon domain and leads to the increase in local rainfall. The indirect effect warms the ocean, which heats the global atmosphere and increases the moisture in the atmosphere; meanwhile, the ocean warming leads to higher temperature increase in the upper troposphere than that in the lower troposphere over East Asia, which weakens the moisture convergence and results in the decrease in Asia monsoon rainfall in the boreal summer.

However, studies of TP SH response to increasing CO₂ are relatively rare. From present cognition on the response of the TP climate to increasing CO₂, it is hard to project the SH response. First, under a global warming scenario, the TP surface may become warmer than that in the present climate (Su et al. 2013), which may contribute to an increase in TP SH. Second, the cloud cover tends to increase in a warming climate (Su et al. 2013). It reduces the solar radiation arriving at TP surface, leads to less solar radiation absorbed and does not favor the increase in SH. Third, the snow cover over the TP may reflect the solar radiation arriving at the surface. If snow cover changes in a warming climate, the reflection and absorption of the solar radiation, as well as surface–air temperature difference, at the TP surface may change. The change in wind speed, which is also a component affecting the SH, is not clear over the TP if CO₂ is increasing. Besides, the increasing CO₂ concentration in atmosphere may induce physiological forcing, which may lead to changes in snow-albedo feedback, as well as temperature changes (Boucher et al. 2009). Therefore, it is necessary to study the SH

response over the TP. In light of the distinct responses of Asia monsoon rainfall to direct and indirect CO₂ effects, the study of direct and indirect CO₂ effects on the TP SH is an interesting topic. It contributes to the understanding of involved dynamics and the thermodynamic processes.

The rest of the paper is organized as follows: Sect. 2 introduces the data and methods; Sect. 3 investigates the annual cycle of the SH changes over the TP; Sect. 4 investigate the SH changes and associated mechanisms during November–April over the TP; Sect. 5 explores the transient change of NDJFMA-averaged SH over the TP in the 1%CO₂ experiment; and Sects. 6 and 7 present the discussion and summary, respectively.

2 Data and methods

The present study is based on monthly outputs of CMIP5 models (Taylor et al. 2012). Table 1 lists information on the CMIP5 models participating in this manuscript. The experiments used are (1) 1% to quadruple CO₂ experiment, in which the models are forced by CO₂ increasing 1% per year until the CO₂ concentration is quadruple. (2) amip experiment, in which the models are run with observed SST, sea ice, anthropogenic and natural forcing from 1979 to 2008; (3) amip4K experiment, which is the same as the amip experiment except the forcing SST is added by 4K; (4) amipFuture experiment, which is the same as the amip experiment except the forcing SST is derived from the multimodel ensemble (MME) mean of 1% to quadruple CO₂ experiment of the Couple Model Intercomparison Project phase 3 models; (5) amip4xCO₂ experiment, which is the same as the amip experiment except the CO₂ concentration being quadruple what it was from 1979 to 2008; (6) historical experiment, in which the models are forced by observed anthropogenic and natural forcings from the mid-19th century to 2005; (7) RCP85 experiment, in which the models are forced by gradually increased radiative forcing that stabilizes at 8.5 W m⁻² after 2100 (Riahi et al. 2011; Vuuren et al. 2011). Only the “r1i1p1” run of the CMIP5 results are analyzed. The models participating in the calculation associated with experiments 1 are bcc-csm1-1, CanESM2, CCSM4, CNRM-CM5, HadGEM2-ES, IPSL-CM5A-LR, IPSL-CM5B-LR, MIROC5, MPI-ESM-LR, MPI-ESM-MR and MRI-CGCM; in experiment 2–4, the outputs of bcc-csm1-1, CanAM4, CCSM4, CNRM-CM5, HadGEM2-A, IPSL-CM5A-LR, IPSL-CM5B-LR, MIROC5, MPI-ESM-LR, MPI-ESM-MR and MRI-CGCM3 are used (CanAM4 and HadGEM2-A are the corresponding atmospheric general circulation models of CanESM2 and HadGEM2-ES, respectively). The surface wind data in bcc-csm1-1 and CCSM4 are absent. The snow cover data in CCSM4, HadGEM2-ES (HadGEM2-A), IPSL-CM5A-LR and IPSL-CM5B-LR are unavailable. The snow melt data in CCSM4, HadGEM2-ES

Table 1 Information on the climate models

Model ID	Availability (Y indicates that the data are available. \ indicates unavailable)						Numbers of grid (elevation no less than 3000 m)
	Historical	RCP85	Amip	Amip4K	AmipFuture	Amip4xCO2	
bcc-csm1-1	Y	Y	Y	Y	Y	Y	33
CanESM2	Y	Y	\	\	\	\	33
CanAM4	\	\	Y	Y	Y	Y	33
CCSM4	Y	Y	Y	Y	Y	Y	228
CNRM-CM5	Y	Y	Y	Y	Y	Y	130
HadGEM2-ES	Y	Y	\	\	\	\	112
HadGEM2-A	\	\	Y	Y	Y	Y	112
IPSL-CM5A-LR	Y	Y	Y	Y	Y	Y	37
IPSL-CM5B-LR	Y	Y	Y	Y	Y	Y	37
MIROC5	Y	Y	Y	Y	Y	Y	130
MPI-ESM-LR	Y	Y	Y	Y	Y	Y	77
MPI-ESM-MR	Y	Y	Y	Y	Y	Y	77
MRI-CGCM3	Y	Y	Y	Y	Y	Y	209

(HadGEM2-A), IPSL-CM5A-LR, IPSL-CM5B-LR and MRI-CGCM3 are unavailable. Besides, NCEP-DOE AMIP-II reanalysis (Kanamitsu et al. 2002) is used to understand the associated changes in observation.

To facilitate the MME study, we used a bilinear interpolation technique to interpolate the data onto a $1.0^\circ \times 1.0^\circ$ grid. Note that the interpolation was not performed when we computed the area average of the data. When the MME was performed, all the available data participated in the computation.

The total response to CO_2 increase is the difference between the climatology during year 121–140 and that during year 1–20. For conciseness, we name the response “1%CO2”. The role of uniform (nonuniform) SST, denoted “4K” (“4K + pattern”), is represented by the difference between the amip4K (amipFuture) and amip experiments. Note that the prescribed patterned SST warming is not identical to multimodel-mean simulated SST warming pattern in 1%CO2 results. It is used to detect the indirect effect of CO_2 . The direct effect of CO_2 is represented by the difference between the amip4xCO2 and amip experiments. This direct effect is named “4xCO2” for convenience. In experiments 2–5, the results of 1979–2008 are studied.

To fairly compare the results of 1%CO2 and amip-associated experiments (experiments 2–5 in the first paragraph of this section), some results are scaled into the same global SST or CO_2 change. We named the global mean SST change in 1%CO2, 4K and 4K + pattern results “ $\text{SST}_{1\%CO_2}$ ”, “ SST_{4K} ” and “ $\text{SST}_{4K+pattern}$ ”. The $\text{SST}_{1\%CO_2}$, SST_{4K} and $\text{SST}_{4K+pattern}$ of the models are displayed in Table 2. To understand the contribution of SST warming to “1%CO2”, the 4K results in each model are multiplied by $\text{SST}_{1\%CO_2}/\text{SST}_{4K}$ in order to normalize the global SST changes of 4K and 1%CO2 to the same level. Similarly, the “4K + pattern” results in each

Table 2 the global mean SST changes, unit: K

Model ID	1%CO2 $\text{SST}_{121-140}$ SST_{1-20}	amip4K-amip	amipFuture-amip
bcc-csm1-1	3.16	4.07	4.14
CanESM2 (CanAM4)	3.79	3.97	4.09
CCSM4	2.98	4.8	4.17
CNRM-CM5	3.65	4.02	4.01
HadGEM2-ES (HadGEM2-A)	3.78	4.03	4.12
IPSL-CM5A-LR	3.65	4.06	3.90
IPSL-CM5B-LR	2.78	4.12	4.20
MIROC5	2.68	4.09	4.14
MPI-ESM-LR	3.35	3.95	4.08
MPI-ESM-MR	3.30	3.95	3.93
MRI-CGCM3	3.05	4.09	4.17

model are multiplied by $\text{SST}_{1\%CO_2}/\text{SST}_{4K+pattern}$. The multiplied “4K + pattern” results minus the multiplied “4K” results denotes the role of “Pattern”. Followed Endo et al. (2018), the 4xCO2 results are multiplied by $\ln(3.3)/\ln(4)$, so that the CO_2 -induced radiation change is the same as 1%CO2. The scaling is widely used in former studies (e.g. Endo et al. 2018; Huang et al. 2013; Kamae et al. 2016). In addition, the 1%CO2 results minus the sum of scaled “4K + pattern” and “4xCO2” results is the role of “Residual” term (Kamae et al. 2016).

3 SH response to CO_2

The SH change in 1%CO2 displays a prominent annual cycle. Figure 2 displays the corresponding SH change in each calendar month. In January, February, March, April,

November and December, the TP is dominated by enhanced SH, with good model agreement (Fig. 2a–d, k, i). The largest enhancement (maximum increase of approximately 22 W m⁻²) occurs southwest of the TP in May. In June, the SH change features a dipole pattern, with increase over the western and southern TP and decrease over the northeastern TP (Fig. 2f). The SH response in May displays a transitional similar pattern from April to June (Fig. 2e). In July, the SH decreases over central north TP and increases over other regions (Fig. 2g). In August and September, the changes in TP SH feature a tripole pattern, with intensified SH over the eastern and western TP and weakened SH over the central TP (Fig. 2h, i). In October, the TP SH response is relatively weak, exhibiting a transitional distribution from September to November (Fig. 2j).

In each model, we counted the number of grids with elevations no less than 3000 m. The numbers are listed in the

rightmost column of Table 1. For bcc-csm1-1, CanESM2, CanAM4, IPSL-CM5A-LR and IPSL-CM5B-LR, no more than 40 grids are higher than 3000 m. The small samples make it difficult to discuss nonuniform change over the TP. If we do not take these models into consideration, the number of models is relatively lacking. For example, if excluding the models with relatively coarse grids, only seven models are left when we discuss the 4K results. Thus, the nonuniform change, especially the SH change during boreal summer, is not our main focus.

Figure 3 displays the averaged SH response at the grids with elevations no less than 3000 m over the TP. The averaged SH change features a distinct annual cycle, consistent with Fig. 2. In the 1%CO₂ results, the averaged SH peaks in April and is the lowest in September. However, the SH changes in 1%CO₂ results in all the months is insignificant except November and December.

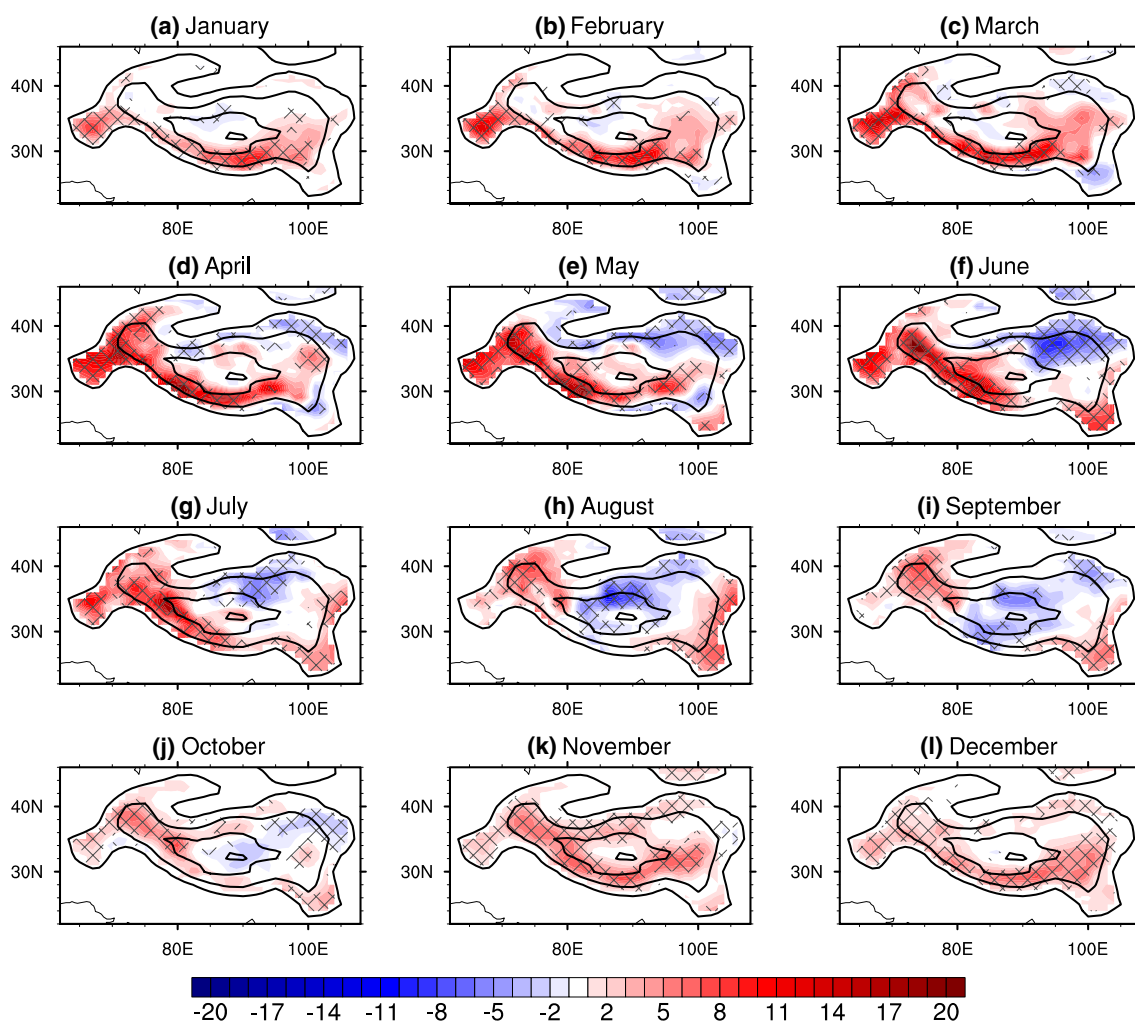


Fig. 2 The SH responses (color shading) for the 1%CO₂ results in each calendar month. The units are W m⁻². The responses are the MME results. The contours represent elevations of 1500 m, 3000 m,

5000 m and 6000 m. The lattices indicate that no less than 2/3 of the models show the same sign response

The amip experiments show that the SH change over the TP from November to April under 1%CO₂ is mainly contributed by the CO₂ indirect effect. In Fig. 3, the contributions of uniform SST, SST pattern, CO₂ radiation and residual terms are plotted. In January, February, March, April, November and December, the SH change in 1%CO₂ is mainly contributed by the uniform SST change. If the SST pattern is taken into consideration, the contribution drops. It means that the SST pattern leads to a decrease in SH over the TP. The contribution of the CO₂ radiation effect is tiny in February, March and April; it is close to the contribution of SST pattern in November, December and January. The contribution of residual term is overall tiny.

From May to September, the contribution of residual terms is the largest among the terms. In May, June and October, the term contributing second largest is SST pattern. In July and August, the second largest contributing term is CO₂ radiative effect. In September, the corresponding term is uniform SST. In general, the feature in these months is inconsistent.

Therefore, in January, February, March, April, November and December (hereafter NDJFMA), the SH changes over TP is relatively uniform; and the features of contribution of uniform SST, SST pattern, CO₂ radiation and residual term are similar. The following sections mainly discuss the SH change from November to April. The results from May to October is not our focus in this paper.

4 NDJFMA responses

On the TP SH in 1%CO₂ results, its increases in NDJFMA share similar features (Figs. 2, 3). Figure 4 displays the response of SH, surface–air temperature difference (surface temperature minus 2 m temperature) and surface

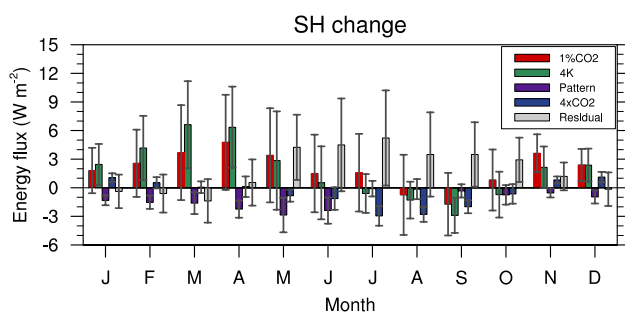


Fig. 3 The averaged SH change over the TP in each calendar month. The red, green, purple, blue and gray bars indicate the 1%CO₂, 4K, pattern, 4xCO₂ and residual results, respectively. The units are W m⁻². Only the grids with elevations no less than 3000 m are used when we compute the average. The error bars denote the 95% confidence intervals of the changes based on intermodel spread. The results of 4K, pattern, 4xCO₂ are scaled so that they can be compared with the results of 1%CO₂

(10 m) wind speed in 1%CO₂ results during NDJFMA. In 1%CO₂ results, the NDJFMA averaged SH mainly increase south of the TP, with a maximum of 10.4 W m⁻². Two factors mainly affect the SH change: the surface–air temperature difference and surface wind speed. The increase in surface–air temperature difference bears resemblance to that in SH (Fig. 4f). The pattern correlation coefficient between changes in surface–air temperature difference and SH is 0.74 over the domain [22°–46°N, 62°–108°E]. The surface wind speed features a decrease over most parts of the TP, but there is an increase over the southeast and northeast TP. Over the area [22°–46°N, 62°–108°E], the pattern correlation coefficient between changes in surface wind speed and SH is -0.27. The surface–air temperature difference makes a positive contribution to the SH increase over the TP, while the surface wind speed makes a generally negative contribution. The increase in SH over the TP indicates that the contribution of the surface–air temperature difference is dominant.

The SH increase over the TP in 1%CO₂ results is mainly contributed by the indirect effects of CO₂. In 4K results, the enhancement of SH is found south of the TP, with a maximum of 14.6 W m⁻² (Fig. 4b). The pattern correlation coefficient between the SH change in 1%CO₂ and 4K results is 0.84 over the domain [22°–46°N, 62°–108°E]. Similar to 1%CO₂ results, the SH change over the TP in 4K results is mainly contributed by changes in surface–air temperature rather than surface wind (Fig. 4g, l).

The SST pattern makes the opposite-sign contribution to the SH increase in 1%CO₂ results over the TP (Fig. 4c). Compared with uniform SST increase, the magnitude of the contribution is weak. The maximum decrease of SH is over southwest of the TP (~3.7 W m⁻²). In pattern results, the pattern correlation coefficient between the change of the SH and the surface–air temperature is 0.84 over the domain [22°–46°N, 62°–108°E]; while, the pattern correlation coefficient between the change of the SH and the surface wind speed is -0.62 over that domain. It indicates that surface–air temperature change is mainly responsible for the SH change in pattern results.

Compared with uniform SST increase, the contribution of direct CO₂ (radiation) effect on SH change in 1%CO₂ is weak (Fig. 4d). The CO₂ radiative effect generally leads to weak increase in the SH over the TP except southeast of the TP. The maximum increase is 3.0 W m⁻². In 4xCO₂ results, the responses of surface–air temperature difference and surface wind speed are also quite small relative to the magnitudes of those in 1%CO₂ and 4K results (Fig. 4d, i, n).

Alike the effect of SST pattern, the effect of residual terms on mean SH change over the TP is weak (Fig. 4e). In residual results, the SH features a tripole change, with increase in the west and east TP and decrease in the central TP. The overall SH above 3000 m weakly decreases (Fig. 3).

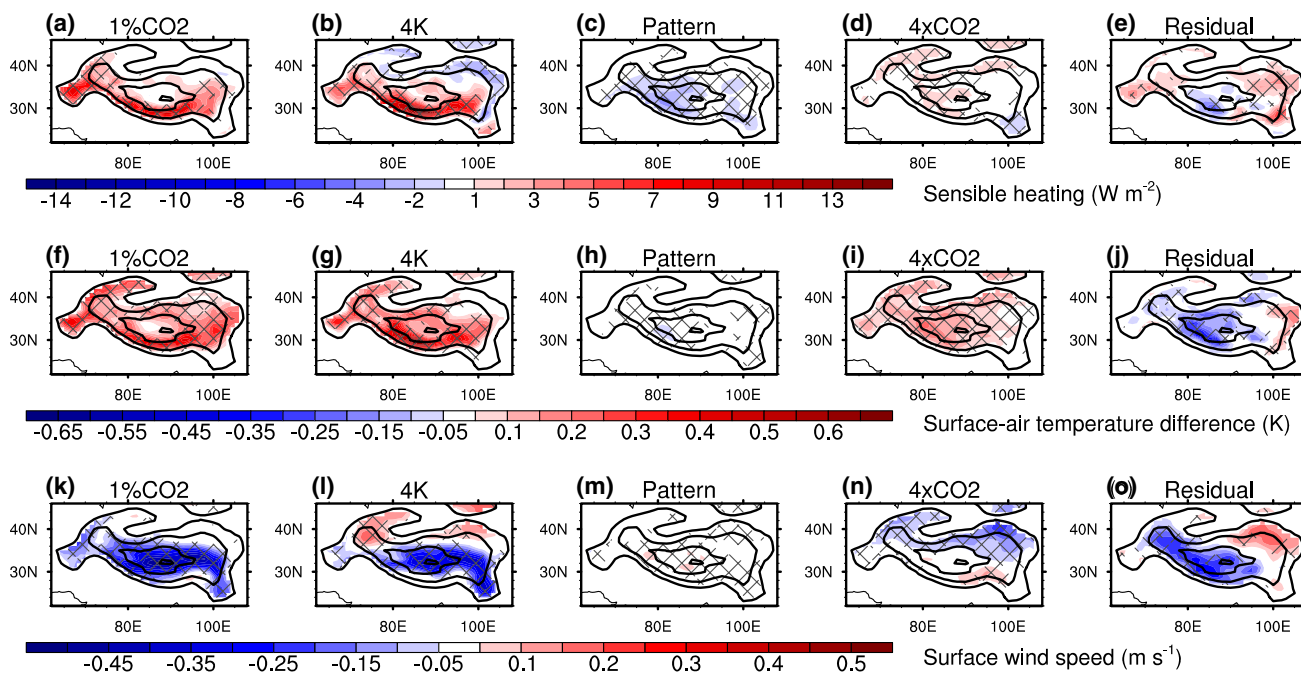


Fig. 4 The NDJFMA-averaged responses (color shading) of SH (top row, units: $W m^{-2}$), surface–air temperature difference (middle row, units: K) and 10 m wind speed (bottom row, units: $m s^{-1}$) in 1%CO₂ (leftmost column), 4K (2nd column), pattern (3rd column), 4xCO₂ (4th column) and residual (rightmost column) results. The responses

are the MME results. The contours demonstrate the elevations of 1500 m, 3000 m, 5000 m and 6000 m. Lattices indicate that no less than 2/3 of the models show the same sign response. The results of 4K, pattern, 4xCO₂ are scaled so that they can be compared with the results of 1%CO₂

The changes in radiation over the TP surface may help in understanding the change in the surface–air temperature difference. Figure 5 displays the changes in TP surface energy flux (downwards solar radiation, upwards solar radiation, downwards longwave radiation, upwards longwave radiation, sensible heat and latent heat) in 1%CO₂, 4K, pattern, 4xCO₂ and residual results. In 1%CO₂ results, the increased downwards and upwards longwave radiation is generally balanced. For downwards solar radiation, it decreases due to change of cloud and water vapor (figures not shown). The decrease in upwards solar radiation cannot be attribute to the weakening of downwards solar radiation, because the magnitude of decrease of the latter is smaller than that of the former. The net solar radiation warms the TP surface and leads to a surface warmer than the atmosphere. In turn, the SH and latent heat intensify, leading to the balance of all radiation. Most likely, due to the relatively dry condition over the TP surface during NDJFMA, the intensification of SH is a relatively efficient way to balance net solar radiation. Overall, this structure of radiation changes favors the enhancement of surface–air temperature difference as well as the SH.

The uniform SST increase is mainly responsible for the radiation changes in 1%CO₂ results. The radiation responses in 4K results are similar to those in the 1%CO₂ results. Slight differences exist in the downwards longwave radiation. In the 4K results, the increase in downwards longwave

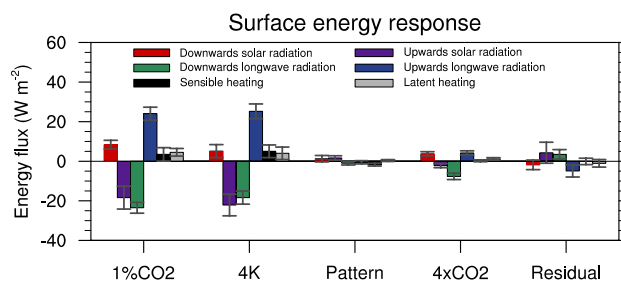


Fig. 5 The NDJFMA-averaged change in each term of the surface radiation in 1%CO₂, 4K, pattern, 4xCO₂ and residual results. Only the grids with elevations no less than 3000 m over the TP participated in the average. Positive and negative indicate heat loss and gain, respectively. The units are $W m^{-2}$. The red, purple, green, blue, black and gray bars denote the downwards solar radiation, upwards solar radiation, downwards longwave radiation, upwards longwave radiation, SH and latent heat, respectively. The error bars represent the 95% confidence intervals of the changes. The results of 4K, pattern, 4xCO₂ are scaled so that they can be compared with the results of 1%CO₂

radiation is slightly weaker than that in the 1%CO₂ results. It is consistent with a larger surface–air temperature difference in the 4K results (Fig. 4e). The effect of other terms (Fig. 5) are relatively small.

The fact that the magnitude of the decrease in upwards solar radiation is larger than that of the decrease in

downwards solar radiation over TP in 1%CO₂ results is consistent with the albedo response. Figure 6a–e displays the albedo change in 1%CO₂, 4K, pattern, 4xCO₂ and residual results. The albedo is the upwards solar radiation divided by downwards solar radiation. In 1%CO₂ results, the whole TP features a decrease in albedo, with maximum magnitude over south TP (~ -0.11). The decrease is mainly contributed by uniform SST increase (Fig. 6b). In 4K results, the whole TP also features a decrease in albedo (maximum decrease approximately 0.15). In both 1%CO₂ and 4K results, the albedo changes are in good agreement among the models. Interestingly, the maximum decrease resides south of the TP, consistent with the maximum changes in surface–air temperature difference and SH in both the 1%CO₂ and 4K results (Fig. 4a, b, f, g). The SST pattern and residual term favors the increase in the albedo over the TP, but the contributions are relatively small (Fig. 6c, e). The contribution of CO₂ radiative effect is negligible (Fig. 6d). The albedo results imply that the albedo may lead to that kind of solar radiation change.

As the snow cover largely affects the albedo, the snow cover is investigated. Figure 6f–j display the responses of snow cover over the TP. In the 1%CO₂ and 4K results, the TP surface is dominated by the shrinkage of snow cover, with maximums of 25% and 31%, respectively. Alike the albedo results, the maximum reduction resides south of the TP, consistent with the maximum changes in surface–air temperature difference and SH in both the 1%CO₂ and 4K results (Fig. 4a, b, f, g).

The snow cover change is mainly determined by the change of snowfall and snowmelt. In 1%CO₂ results, slightly increased snowfall occurs above 3000 m over the TP and decreased snowfall is found near south edge of

the domain with elevation above 3000 m (Fig. 7a). Above 3000 m over the TP, the temperature is cold enough, the fraction of precipitation that falls as snow changes little, while the increase in temperature increases the moisture as well as the precipitation and snowfall. Over south edge of the domain with elevation above 3000 m, the surface temperature transits from below to above 0 °C (the green and red contours in Fig. 7a), leading to a reduction of fraction of the total precipitation falling as snow. It shares the same mechanism proposed by Krasting et al. (2013). The pattern of snowmelt change is similar to that of snowfall in 1%CO₂ results (Fig. 7f). Under warmer climate, above 3000 m over the TP, increased precipitation provides more available snow to melt and higher temperature leads to the more likelihood of snow to melt; while, over south edge of the domain with elevation above 3000 m, the decreased snowmelt is results from the reduction of precipitation or snowfall. The explanation is enlightened from McCabe and Wolock (2010). The net effect of snowfall and snowmelt is towards a decrease in snow cover over the entire TP (Figs. 6f, 7k). The maximum of net snow loss is south of the TP, probably due to the transition of local temperature from above to below 0 °C and the large snow cover.

For the changes associated with snow, uniform SST increase is mainly responsible. The patterns of the change of snow cover, snowmelt and difference between snowfall and snowmelt in 4K results are similar to those of 1%CO₂ results (Figs. 6f, g, 7f, g, k, l). The snowfall in 4K results is similar to that in 1%CO₂ results over south edge of the domain with elevation above 3000 m; while, above 3000 m, the snowfall slightly decreases in 4K and slightly increase in 1%CO₂. It is probably led by larger reduction of temperature in 4K results than 1%CO₂ results (the green and red contours in

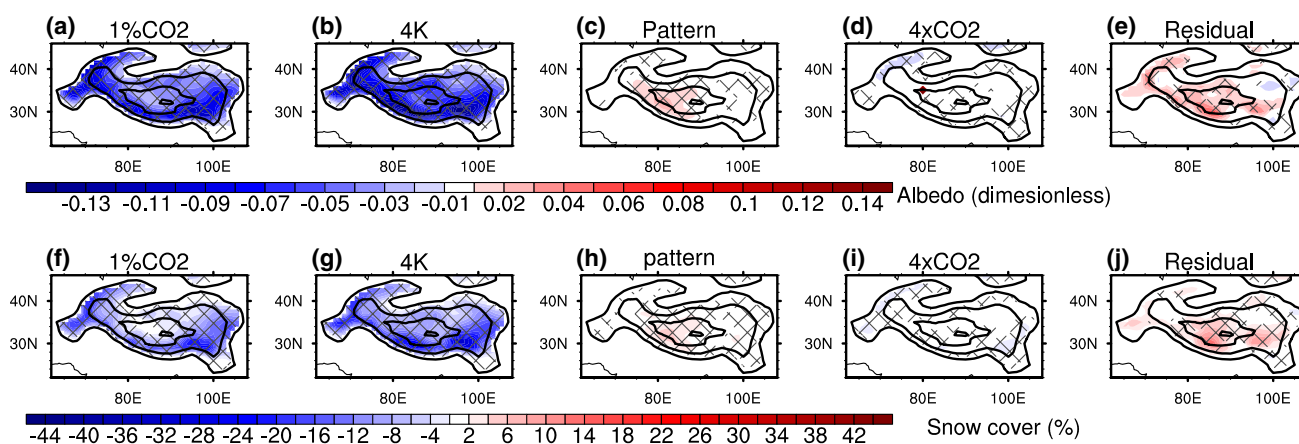


Fig. 6 The NDJFMA-averaged responses (color shading) of albedo (top row, units: %) and snow cover (bottom row, units: K) in 1%CO₂ (leftmost column), 4K (2nd column), pattern (3rd column), 4xCO₂ (4th column) and residual (rightmost column) results. The albedo is the upwards solar radiation divided by downwards solar radiation.

The response is the MME results. The black contours are for elevations of 1500 m, 3000 m, 5000 m and 6000 m. Lattices indicate that no less than 2/3 of the models show the same sign response. The results of 4K, pattern, 4xCO₂ are scaled so that they can be compared with the results of 1%CO₂

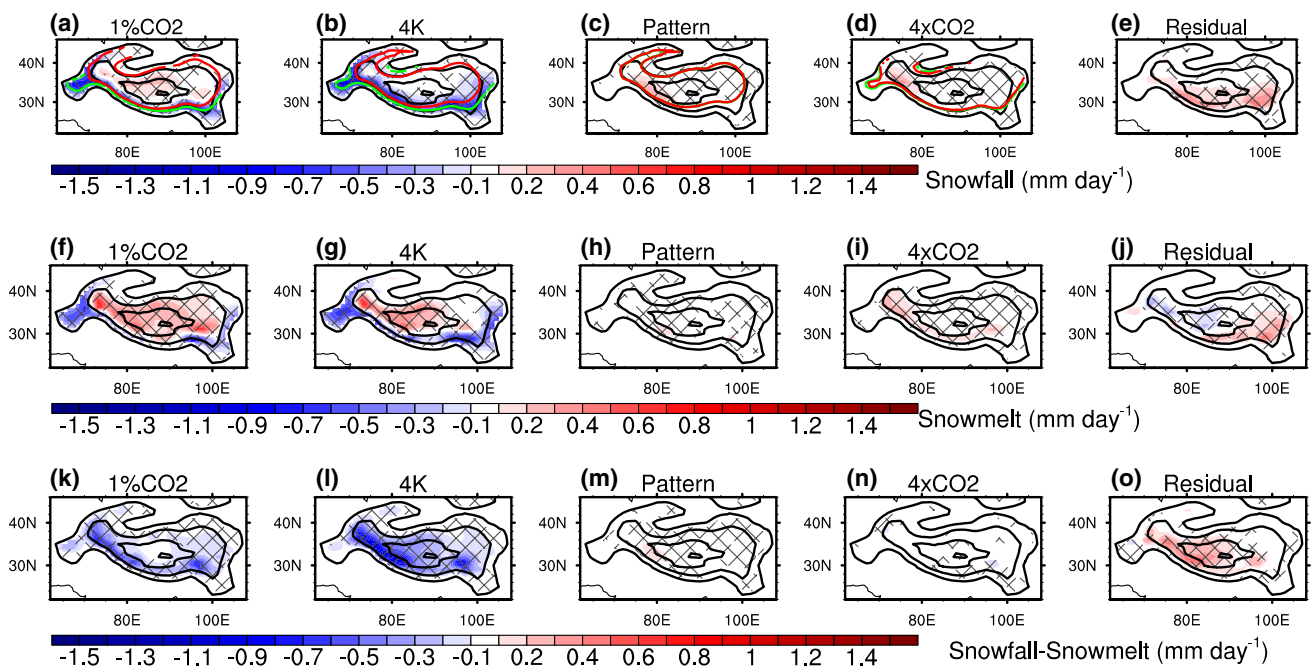


Fig. 7 The NDJFMA-averaged responses (color shading) of snowfall (top row), snowmelt (middle row) and the difference between snowfall and snowmelt (bottom row) in 1%CO₂ (leftmost column), 4K (2nd column), pattern (3rd column), 4xCO₂ (4th column) and residual (rightmost column) results. The units are mm day⁻¹. The response is the MME results. The black contours are for elevations of 1500 m, 3000 m, 5000 m and 6000 m. The green contours in **a–d** are the 0 °C contours of the climatological surface temperatures in

the first 20 years of 1%CO₂ experiment, amip experiments, amip4K experiments and amip experiments, respectively. The red contours in **a–d** are the 0 °C contours of the climatological surface temperatures in the years 121–140 of 1%CO₂ experiment, amip4K experiments, amipFuture experiments and amip4xCO₂ experiments, respectively. Lattices indicate that no less than 2/3 of the models show the same sign response. The results of 4K, pattern, 4xCO₂ are scaled so that they can be compared with the results of 1%CO₂

Fig. 7a, b). For the changes of snow cover, snow melt and their difference, the contribution of residual terms are the second largest in magnitude, with the opposite sign (Figs. 6j, 7j, o). While, the residual terms act to slightly increase the snowfall above 3000 m (Fig. 7e). The contribution of pattern and CO₂ radiative effect is negligible to the snow associated changes (Figs. 6i, 7d, i, n).

The insulating effect of snow contributes to the good agreement of snow cover change with the SH change. The TP, even the south TP, is not entirely covered by snow or ice. For the area which is not covered by snow or ice, the SH is mainly affected by surface–air temperature difference; for the area covered by snow or ice, the SH exchange is insulated.

Soil moisture enlarges the response over south of the TP in 1%CO₂ and 4K results. The local soil moisture is decreasing (figure not shown), which may enlarge the local temperature increase. It induces stronger snow-albedo feedback and finally leads to larger enhancement of local SH increase.

Therefore, for SH increase in NDJFMA over the TP, the effect of uniform SST increase is mainly responsible. Increasing CO₂ may lead to SST warming, which warms the atmosphere, including the atmosphere over the TP. Consequently, over the TP, the shrinkage of snow cover benefits

the absorption of downwards solar radiation and increases the surface–air temperature difference. This increase in surface–air temperature difference leads to the increase in SH. Changes in surface wind speed have little effect on SH.

5 The transient response

Somewhere in the TP, the surface is rather cold climatologically. If the temperature increase is inadequate, the snow cover rarely changes. The changes in SH as well as surface–air temperature difference and snow may be nonlinear versus the environmental temperature increases. In the light, it is necessary to check whether this nonlinear process influences the aforementioned responses in Sects. 3 and 4. However, the transient changes in the variables indicate that the area-averaged responses over the TP are generally linear (Fig. 8), at least above elevations of no less than 3000 m.

The NDJFMA-averaged SH as well as surface–air temperature difference display a prominent increasing trend during the 21st century in 1%CO₂ experiment (Fig. 8a, c). The NDJFMA snow cover shows a decreasing trend (Fig. 8b). The above trends further prove the thought that the snow

cover-induced change in surface–air temperature difference is mainly responsible for the SH change over the TP.

Why is the nonlinear change not found in transient changes in snow cover over the TP? That behavior may be associated with calculation of the area average. In the present study, the area average is performed on the grids with elevations no less than 3000 m. During NDJFMA, south of the TP, the MME 0 °C contours of climatological surface temperature roughly reside at 3000 m in both year 1–20 of 1%CO₂ experiment and amip experiments (the green contours in Fig. 7a, b). As the atmosphere warms, the area with surface temperatures below 0 °C gradually retreats above 3000-m elevation. In general, it results in the fact that the area average of the snow cover over the TP decreases linearly rather than abruptly versus temperature increase. Thus, the surface–air temperature difference and the SH vary nearly

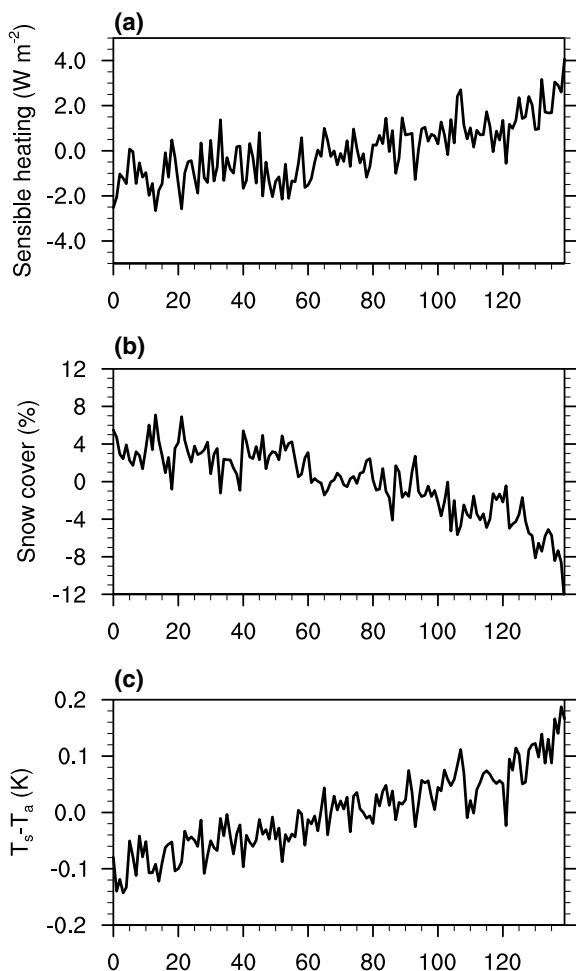


Fig. 8 The transient changes of the NDJFMA-averaged SH (top row, units: W m^{-2}), snow cover (middle row, units: %) and surface–air temperature (bottom row, units: K) in 1%CO₂ experiment. To facilitate the comparison, all the results are subtracted by the average during 2006–2099. The results are the MME results of the CMIP5 models

linearly as climate gradually warms. If the participating grids are no less than 5000 m or higher, the nonlinearity of the transient changes is more apparent (figures not shown). However, if the grids with elevations no less than 5000 m are considered in area averages, the number of participating grids in some models may be low.

6 Discussion

The study of 1%CO₂ favors the understanding of the TP SH response in RCP85 scenario. Figure 9 displays the TP-averaged SH response in each calendar months in RCP85, 4K, pattern, 4xCO₂ and residual results, respectively. Here, the RCP85 results is the average of RCP85 during 2080–2099 minus the average of historical simulation during 1980–2005. Only the grids with elevations no less than 3000 m are participating in the calculation. Alike the 1%CO₂ results, the results of 4K, pattern and 4xCO₂ are scaled. As the aerosols varies in RCP85 scenario relative to historical simulation, it alters the global mean SST change (Xie et al. 2013). Consequently, the contribution of uniform SST change and SST pattern to the TP SH responses is slightly different to those in 1%CO₂ results (Fig. 9). Another apparent difference is the contribution of the residual terms. In 1%CO₂ results, during NDJFMA, its contribution to the TP SH is slightly negative; while, in RCP85 scenario, the contribution is positive. It implies that the aerosols radiative effect favors the increase in TP SH during NDJFMA. But the lack of similar amip-type simulation assessing the aerosol effect makes it difficult to fairly compare its role with the effects of SST change and CO₂ directly radiative effect.

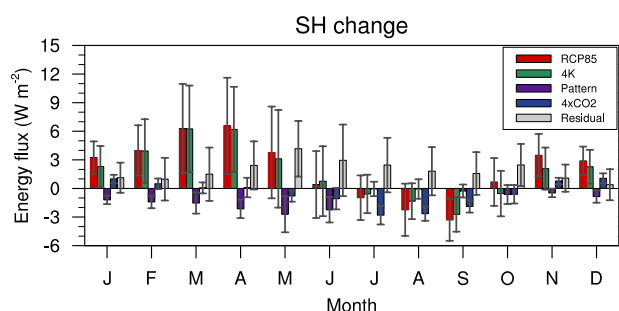


Fig. 9 The averaged SH change over the TP in each calendar month. The red, green, purple, blue and gray bars indicate the RCP85, 4K, pattern, 4xCO₂ and residual results, respectively. The units are W m^{-2} . Here, the RCP85 results is the average of RCP85 during 2080–2099 minus the average of historical simulation during 1980–2005. Only the grids with elevations no less than 3000 m are used when we compute the average. The error bars denote the 95% confidence intervals of the changes based on intermodel spread. The results of RCP85, pattern, 4xCO₂ are scaled so that they can be compared with the results of RCP85

In NCEP-DOE AMIP-II reanalysis, an overall decreasing SH trend is found over the TP during NDJFMA from 1979 to 2006 (Fig. 10a). The decreasing trend is more apparently over the east TP. The similar trend of surface–air temperature difference implies that it may mainly account for the SH trends (Fig. 10b). The significantly decreased SH is balanced by upwards solar radiation (Fig. 10f); the trends of other surface energy flux are relatively small (Fig. 10d, e, g, h). During 1970–2006, as the atmosphere becomes wetter, significant increase in snow cover over the east TP is found in satellite data (Wang et al. 2018). It is consistent to the fact that the magnitude of increase in upwards solar radiation is larger than that of decrease in downwards solar radiation (Fig. 10e, f). Accompanied by the increasing concentration of CO₂ in atmosphere during 1979–2006, the TP SH during NDJFMA, however, is decreasing. It mismatches the finding based on CMIP5 simulations of present study. This mismatch is probably led by the aerosol or internal variability of climate system.

In the present investigation, the diagnostic analysis is not employed due to the drag coefficient for heat. The SH is the product of the coefficient, the air density, the specific heat of dry air at constant pressure, surface wind speed and surface–air temperature difference. The drag coefficient for heat is not constant over the TP and differs among studies (Duan and Wu 2010; Yeh and Wu 1998). More importantly, we are not able to obtain the coefficient in the models. It makes it difficult to fairly compare the contributions of individual factors with model results using diagnostic analysis. Using fractional change may avoid the uncertainty of drag coefficient for heat, a new problem comes out: over the areas where the surface–air temperature difference is tiny, the fractional changes are exaggerated (figure not shown). This is also not

quite straightforward to compare the contributions. Thus, it seems that there is no good way to diagnose the contribution of surface–air temperature difference and wind speed in CMIP5 results.

In addition, the reduction of snow cover may favor the elevated heating of the TP. Simulation of a cloud system-resolving model revealed that in present-day climate, the elevated heating of the TP is compensated by the surface albedo increase with elevation (Hu and Boos 2017). In response to CO₂ increasing, the surface albedo over the TP may reduce. The albedo increase with elevation will be weaker than that in present-day climate. It implies that the thermal forcing of the TP will be more apparent under global warming.

7 Summary

Using a set of CMIP5 experiments, the present study investigates the TP SH response to increasing CO₂ as well as the contributions of the CO₂ direct and indirect effects to the response. In the 1%CO₂ results, the TP features enhanced SH, with good model agreements in January, February, March, April, November and December. In June, the SH change nearly features a dipole pattern, with increase over the western and southern TP and decrease over the northeastern TP. In July the SH decreases over central north TP and increases over other regions. In August and September, the TP features a tripole pattern (increase over the eastern and western TP but decrease over the central TP). The SH changes in May and October, however, display a transitional pattern between the nearby 2 months. According to the pattern and the averages of the SH response, the changes in January, February, March,

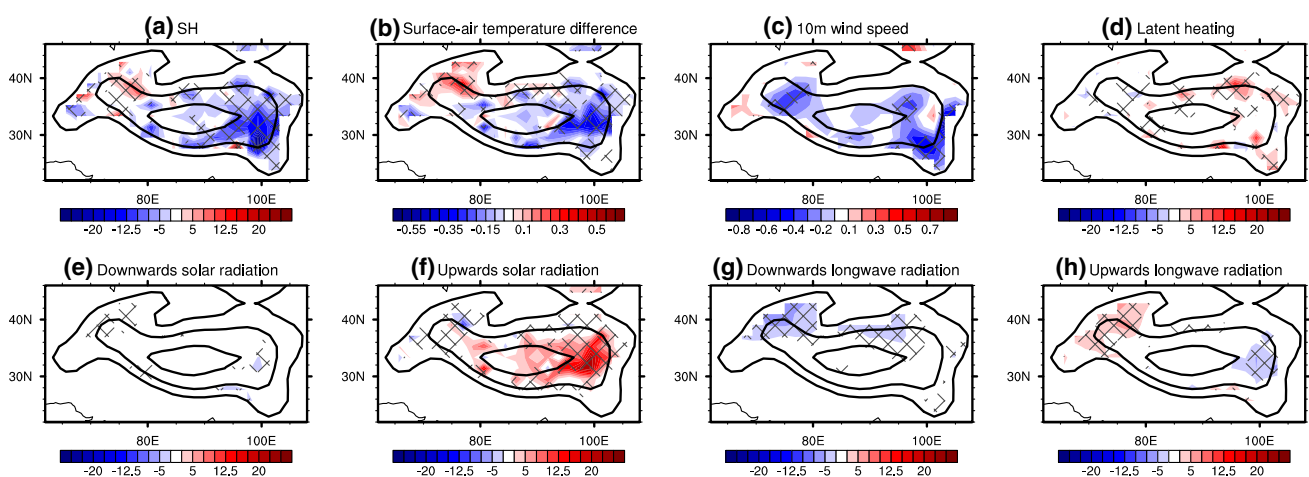


Fig. 10 The trend of the SH (a), surface–air temperature difference (b), 10 m wind speed (c), latent heating (d), downwards solar radiation (e), upwards solar radiation (f), downwards longwave radiation (g) and upwards longwave radiation (h) during 1979–2006 in NCEP-

DOE AMIP-II reanalysis. The units in a, d–h are $\text{W m}^{-2} \text{decade}^{-1}$; the unit in b is K decade^{-1} ; the unit in c is $\text{m s}^{-1} \text{decade}^{-1}$. The black contours are for elevations of 1500 m, 3000 m, 5000 m and 6000 m. Lattices indicate that the trends exceeding 95% significance level

April, November and December share the same features. Thus, the NDJFMA-averaged SH change over the TP is the focus of the article.

During NDJFMA, SH mainly enhanced south of the TP. The uniform SST increase led by CO₂ increasing is mainly responsible for the enhancement. The increased concentration of CO₂ may lead to the SST warming, which warms the atmosphere above the TP. It leads to: (1) reduction in snowfall over the TP, with maximum over south TP; (2) increased snowmelt mainly above 3000 m and decreased snowmelt near or south of 3000 m elevation south of TP. The net effects of snowfall and snowmelt are towards the reduction of the snow cover over the TP. The net snow cover decrease relatively fast south of the TP primarily because the local surface temperature increases from below to above 0 °C. Through the snow-albedo feedback, the decrease in snow cover lead to more downwards solar radiation absorbed by the surface and less solar radiation reflected to atmosphere, intensifies the surface–air temperature difference and enhances the SH. Besides, the decreased snow cover reduces the insulating effect between surface and atmosphere and favors the SH exchange. The contribution of change in surface wind speed on SH is little.

The transient responses of the TP SH from 2006 to 2009 in the 1%CO₂ results are generally linear if only grids with elevations no less than 3000 m participate in the calculation of area average; this is because above 3000 m, the snow cover gradually shrinks as the climate slowly warms, which is reflected in the area averaged results of snow cover. The linear response of TP-averaged snow cover may lead to approximately linear changes in surface–air temperature difference and finally the SH. When only considering the grids above 5000 m in the calculation of the area average, the linearity may be weaker.

The comparison of 1%CO₂ results with RCP85 results and historical results based on NCEP-DOE AMIP-II reanalysis implies that when understanding the change of TP SH in historical or warmer climate, the role of aerosol should not be ignored.

Acknowledgements We acknowledge the World Climate Research Programme's Working Group on Coupled Modelling, which is responsible for CMIP, and we thank the climate modeling groups (listed in Table 1 of this paper) for producing and making available their model output. For CMIP the U.S. Department of Energy's Program for Climate Model Diagnosis and Intercomparison provides coordinating support and led development of software infrastructure in partnership with the Global Organization for Earth System Science Portals." Besides, the authors wish to thank three anonymous reviewers for the insightful comments that lead to a significant improvement to the manuscript. The study was supported by the National Natural Sciences Foundation of China (Grant nos. 41425019, 41831175 and 41530425) and the Strategic Priority Research Program of Chinese Academy of Sciences (XDA20060501).

References

- Bony S, Bellon G, Klocke D, Sherwood S, Fermepein S, Denvil S (2013) Robust direct effect of carbon dioxide on tropical circulation and regional precipitation. *Nat Geosci* 6(6):447–451
- Boos WR, Kuang Z (2010) Dominant control of the South Asian monsoon by orographic insulation versus plateau heating. *Nature* 463(7278):218–222
- Boucher O, Jones A, Betts RA (2009) Climate response to the physiological impact of carbon dioxide on plants in the Met Office Unified Model HadCM3. *Clim Dyn* 32(2–3):237–249
- Duan AM, Wu GX (2010) Weakening trend in the atmospheric heat source over the Tibetan Plateau during recent decades. *J Clim* 21:3149–3164
- Endo H, Kitoh A, Ueda H (2018) A unique feature of the Asian summer monsoon response to global warming: the role of different land–sea thermal contrast change between the lower and upper troposphere. *SOLA* 14:57–63
- Hu S, Boos WR (2017) Competing effects of surface albedo and orographic elevated heating on regional climate. *Geophys Res Lett* 44(13):6966–6973
- Huang P, Xie S-P, Hu K, Huang G, Huang R (2013) Patterns of the seasonal response of tropical rainfall to global warming. *Nat Geosci* 6(5):357–361
- Kamae Y, Watanabe M, Kimoto M, Shiogama H (2014) Summertime land–sea thermal contrast and atmospheric circulation over East Asia in a warming climate—part II: importance of CO₂-induced continental warming. *Clim Dyn* 43(9–10):2569–2583
- Kamae Y, Watanabe M, Ogura T, Yoshimori M, Shiogama H (2015) Rapid adjustments of cloud and hydrological cycle to increasing CO₂: a review. *Curr Clim Change Rep* 1(2):103–113
- Kamae Y, Ogura T, Watanabe M, Xie SP, Ueda H (2016) Robust cloud feedback over tropical land in a warming climate. *J Geophys Res Atmos* 121(6):2593–2609
- Kanamitsu M, Ebisuzaki W, Woollen J, Yang SK, Hnilo JJ, Fiorino M, Potter GL (2002) NCEP-DOE AMIP-II reanalysis (R-2). *Bull Am Meteorol Soc* 83(11):1631–1643
- Krasting JP, Broccoli AJ, Dixon KW, Lanzante JR (2013) Future changes in Northern Hemisphere snowfall. *J Clim* 26(20):7813–7828
- Lee JY, Wang B, Seo KH, Ha KJ, Kitoh A, Liu J (2015) Effects of mountain uplift on global monsoon precipitation. *Asia Pac J Atmos Sci* 51(3):275–290
- Li X, Ting M (2017) Understanding the Asian summer monsoon response to greenhouse warming: the relative roles of direct radiative forcing and sea surface temperature change. *Clim Dyn* 49(7–8):2863–2880
- Li C, Yanai M (1996) The onset and interannual variability of the Asian summer monsoon in relation to land–sea thermal contrast. *J Clim* 9(2):358–375
- Li D, Li W, Wei L, Zhong H, Lu L, Ji G (2003) A diagnostic study of surface sensible heat flux anomaly over the Qinghai–Xizang Plateau. *Clim Environ Res* 8(1):71–83 (in Chinese)
- Liu Y, Hoskins B, Blackburn M (2007) Impact of Tibetan orography and heating on the summer flow over Asia. *J Meteorol Soc Jpn* 85:1–19
- Ma J, Xie SP, Kosaka Y (2012) Mechanisms for tropical tropospheric circulation change in response to global warming. *J Clim* 25(8):2979–2994
- McCabe GJ, Wolock DM (2010) Long-term variability in Northern Hemisphere snow cover and associations with warmer winters. *Clim Change* 99(1–2):141–153
- Riahi K, Rao S, Krey V, Cho C, Chirkov V, Fischer G, Kindermann G, Nakicenovic N, Rafaj P (2011) RCP 8.5—a scenario

- of comparatively high greenhouse gas emissions. *Clim Change* 109(1–2):33–57
- Sampe T, Xie SP (2010) Large-Scale dynamics of the Meiyu-Baiu Rainband: environmental forcing by the Westerly Jet. *J Clim* 23(1):113–134
- Shaw TA, Voigt A (2015) Tug of war on summertime circulation between radiative forcing and sea surface warming. *Nat Geosci* 8(7):560–566
- Sherwood SC, Bony S, Boucher O, Bretherton C, Forster PM, Gregory JM, Stevens B (2015) Adjustments in the forcing-feedback framework for understanding climate change. *Bull Am Meteorol Soc* 96(2):217–228
- Stocker TF, Qin D, Plattner GK, Alexander LV, Allen SK, Bindoff NL, Bréon FM, Church JA, Cubasch U, Emori S (2013) Technical summary. In: Stocker TF, Qin D, Plattner G-K et al (eds) *Climate change 2013: the physical science basis. Contribution of working group I to the fifth assessment report of the intergovernmental panel on climate change*. Cambridge University Press, Cambridge, p 180
- Su F, Duan X, Chen D, Hao Z, Cuo L (2013) Evaluation of the global climate models in the CMIP5 over the Tibetan Plateau. *J Clim* 26(10):3187–3208
- Taylor KE, Stouffer RJ, Meehl GA (2012) An overview of CMIP5 and the experiment design. *Bull Am Meteorol Soc* 93(4):485–498
- Vuuren DPV, Edmonds J, Kainuma M, Riahi K, Thomson A, Hibbard K, Hurtt GC, Kram T, Krey V, Lamarque JF (2011) The representative concentration pathways: an overview. *Clim Change* 109(1–2):5–31
- Wang B, Ding Q (2008) Global monsoon: dominant mode of annual variation in the tropics. *Dyn Atmos Oceans* 44(3–4):165–183
- Wang X, Yang M, Wan G (2013) Temporal-spatial distribution and evolution of surface sensible heat flux over Qinghai–Xizang Plateau during last 60 years. *Plateau Meteorol* 32(6):1557–1567 (**in Chinese**)
- Wang Z, Wu R, Huang G (2018) Low-frequency snow changes over the Tibetan Plateau. *Int J Climatol* 38(2):949–963
- Wu G, Liu Y, He B, Bao Q, Duan A, Jin FF (2012) Thermal controls on the Asian summer monsoon. *Sci Rep* 2:404
- Xie SP, Lu B, Xiang B (2013) Similar spatial patterns of climate responses to aerosol and greenhouse gas changes. *Nat Geosci* 6:828–832
- Yeh DZ, Wu GX (1998) The role of the heat source of the Tibetan Plateau in the general circulation. *Meteorol Atmos Phys* 67(1–4):181–198
- Zhu L, Huang G, Fan G, Qu X, Zhao G, Hua W (2017) Evolution of surface sensible heat over the Tibetan Plateau under the recent global warming hiatus. *Adv Atmos Sci* 34(10):1249–1262

Publisher's Note Springer Nature remains neutral with regard to jurisdictional claims in published maps and institutional affiliations.